PCCP

Accepted Manuscript

ROYAL SOCIETY OF CHEMISTRY

www.rsc.org/pccp

Journal Name

RSCPublishing

ARTICLE

Contamination-Resistant Silica Antireflective Coating with Closed Ordered Mesopores

Cite this: DOI: 10.1039/x0xx00000x

Jinghua Sun,[ab] Qinghua Zhang,[c] Ruimin Ding,[a] Haibing Lv,[c] HongWei Yan,[c] Xiaodong Yuan*[c] and Yao Xu*[a]

Received 00th January 2012,
Accepted 00th January 2012

DOI: 10.1039/x0xx00000x

www.rsc.org/

Porous silica optical antireflective (AR) coatings prepared by traditional sol-gel method have been extensively used for high power laser system, but a serious drawback is that contamination existed in high vacuum is easily absorbed by the disordered open pore structure, resulting in the fast decrease of transmittance. To improve the stability of transmittance in vacuum, a contamination-resistant silica AR coating with ordered mesopores completely closed by hydrophobic-oleophobic groups was successfully developed on fused quartz substrate. The ordered mesopores in coating were controlled under the direction of surfactant F127 via evaporation-induced-self-assembling process and then were closed by post-grafting long chain fluoroalkylsilane. The grazing incidence small angle X-ray scattering (GISAXS) and the X-ray reflectivity (XRR) results indicated that the mesopores in coating constructed a Fmmm orthorhombic symmetry structure with (010) plane parallel to substrate. Cage-like mesopores were confirmed by nitrogen adsorption/desorption analysis. The obtained coatings showed low surface roughness, excellent abrase-resistance and high transmittance of 100 % on quartz substrate. Especially, the decrease of transmittance tested with polydimethylsiloxane pollution in vacuum within one-month was small as 0.02 %. Laser induced damage threshold was up to 59.8 Jcm^{-2} at 12 ns laser pulse of 1053 nm wavelength. This work provides an alternative way to fabricate AR coating with high stability.

1. Introduction

Antireflective (AR) coatings have been widely used in optical devices to reduce light reflection.[1-3] In high power laser system, a large number of transmissive optical elements with AR coatings have been used. If these transmissive optical elements had not been coated, a reflective loss of as much as 8 % from two optical surfaces would accumulate to a serious extent so that no enough energy could reach the target. Porous silica AR coatings prepared by sol-gel method are the most commonly used coatings because of the excellent transmittance, high laser-induced damage threshold (LIDT), low cost and easy large-volume production.[4-9] Owing to the voids between the particles, the coating prepared from monodispersed colloidal silica suspension by Stöber method[10] has the refractive index as low as about 1.22, close to the square root of the index of fused quartz (1.46), making the transmittance of near 100 %.[11] However, this porous silica AR coating extremely easily adsorbs water and other volatile organic components, which will increase the refractive index of coating, lower the transmittance and LIDT.[12-14] Also another defect of this coating is the weak mechanical performance coming from the weak binding force between silica particles and substrate as well as between particles.[15-17] For these problems, many techniques have been developed, mainly focused on the introduction of hydrophobic groups into coating, including ammonia and hexamethyldisilazane vapor treatment,[18-20] polydimethylsiloxane (PDMS) and methyltriethoxysilane or dimethyldiethoxysilane/tetraethyl orthosilicate (TEOS) co-condensation.[6, 21-26] These methods can effectively hinder water adsorption on porous silica AR coatings in atmospheric environment meanwhile improving the mechanical properties slightly. But high vacuum is the real condition existed in high power laser system, the adsorption of organic pollutants will become more serious on the weakly polar coating surface by adopting above method. Furthermore, the organic contamination in high vacuum of high power laser system is much more complicated than in the atmosphere because many materials,[27,28] such as rubber, wire, lubrication oil and so on, may give out diverse gases with different molecular weight. How to solve this contradiction of porous structure between low refractive index and high stability is a big challenge.

Fortunately, the appearance of ordered mesoporous silica films with controllable uniform pore size provides a new choice for solving above problem,[29-34] because proper ordered mesopores can be closed by appropriate surface modification, the adsorption of volatile organics in coating can be efficiently prevented in vacuum. Compared to amorphous porous coatings, ordered mesoporous coating not only possesses low refractive index, but provides uniform pore size to facilitate closing pore entrance and to improve the environment stability. But until now, the corresponding work is seldom reported for high power

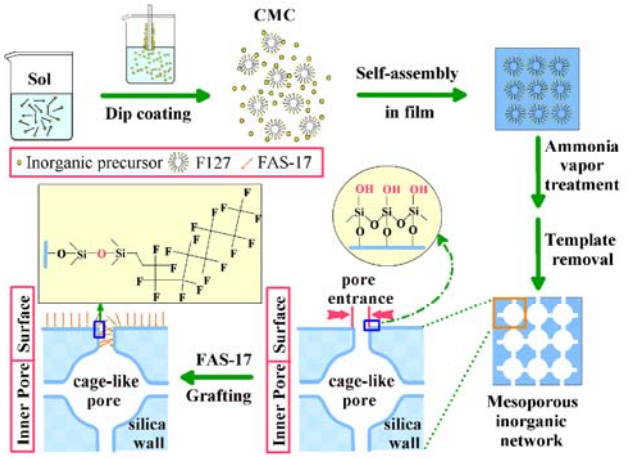

Fig. 1 Schematic illustration of preparation in the ordered cage-like mesoporous silica coatings and the designed closed pore structure posted-grafted by a long chain fluoroalkylsilane molecule (FAS-17).

laser system. Typical SBA-16 mesoporous silica is considered as a very promising structure because it has high porosity, large pore size and uniform cage-like mesoporous connected each other through narrow channels.[35,36] If the pore openings on the surface of cage-like mesoporous silica film are closed through a mild chemical method, the high porosity and the low refractive index would be maintained and organic pollutants be prevented from getting into mesopores.

In this work, considering the structure of SBA-16, a contamination-resistant silica optical AR coating with closed cage-like mesoporous structure have been successfully prepared for high power laser system using TEOS as precursor and Pluronic F127 as template under acidic condition via evaporation-induced-self-assembly process. After thermal treatment, the mesopores were formed in coating, and then the surface pore entrances of coating were closed by 1H, 1H, 2H, 2H-perfluorodecyltriethoxysilane (FAS-17) via post-grafting process. The preparation process can be found in Fig. 1. To enhance the strength of mesoporous matrix, ammonia vapor treatment was carried out before F127 was removed from coating to form ordered mesopores.

2. Experimental

2.1. Coating Preparation.

The coating solution involved in this work was prepared using triblock copolymer surfactant Pluronic F127 as template and tetraethyl orthosilicate (TEOS) as precursor under acidic condition. Pluronic F127 (i.e. OH $(CH_2$-$CH_2O)_{106}(CHCH_3CH_2O)_{70}(CH_2$-$CH_2O)_{106}H$) was obtained from Sigma. TEOS was obtained from Acros (98 %) and Ethanol and hydrochloric acid (HCl) from Beijing Chemical Works.

The sols used for deposition were synthesized using the following preparation. A stock solution of prehydrolyzed silica precursor was prepared by adding (in the following order) TEOS, ethanol, H_2O and HCl =1: 7: 2: 0.006. The sol was left to react under stirring at 60 ^oC for 1.5 h. A second solution was prepared by dissolving different content of F127 in 67.6 ml of Ethanol and 4.5 ml of acid aqueous solution. The final sols, with the molar ratios TEOS and F127 =1: 0.001-0.011, were stirred for 24 h and aged for a week at room temperature. Thin coatings were produced by dip coating at different withdrawal rate on fused quartz substrate. Substrates were cleaned in 1 M HNO_3 for 12 h at room temperature and successively rinsed with water, ethanol and acetone to promote the formation of homogeneous coating and good adhesion. After deposition, as-prepared coatings were dried in air for 24 h and then calcined at 550 °C for 1 h to remove surfactant. Thus-obtained mesoporous silica coatings were F01, F03, F05, F07, F09 and F11 according to the F127 content in solution. F01 and F03 had been abandoned because of their low transmittance. There were many spots on the surface of sample F11 resulting from excessive surfactant content. On the basis of these reasons, we mainly focused on the samples F05, F07 and F09. To stiffen of the silica network, the three samples were left in a saturated ammonia atmosphere for 20 min and underwent the same thermal treatment, which were labeled F05N, F07N and F09N, respectively.

The above-calcined coatings were placed in a closed 500 ml vessel together with a glass container filled with 1 g 1H, 1H, 2H, 2H-perfluorodecyltriethoxysilane (FAS-17, Alfa, 97 %) and this vessel was heated at 150 °C for 1 h in an oven. After that, the vaporization of FAS-17 was stopped and the coatings were baked for 1 h in air at 150 °C. After cooled down to room temperature, the fluoroalkyl-grafted coatings were marked as F05NF, F07NF and F09NF, in that order. To test the antipollution of AR coatings, the ungrafted and fluoroalkyl-grafted ordered mesoporous silica coatings were exposed to polydimethylsiloxane (PDMS) (with an average molecular weight of 115,000 and approximate vapor concentration of 4.036×10^{-7} mol/m^3) vapor at room temperature under a vacuum condition of 10^{-3} Pa for a month.

2.2. Instruments and Characterization.

The ordered structure of the mesoporous coatings was investigated by 2D Grazing incidence small-angle X-ray scattering (GISAXS) experiments, which were performed at BL16B1 beamline of Shanghai Synchrotron Radiation Facility (SSRF) in China. The incidence X-ray wavelength λ was 0.124 nm and the camera length was 2035 mm. The GISAXS test was also carried out at 1W2A beamline of Beijing Synchrotron Radition Facility (BSRF), where the X-ray wavelength was 0.154 nm and the camera length was 1670 mm. A two-dimensional detector with 2048×2048 pixels was used to collect both in- and out-of-plane scattering data. Due to the presence of an intense specular beam at grazing angles of incidence, lead strips were used to attenuate the scattering along the specular plane. The incident angle of primary beam to sample surface was chosen at 0.2°, just above the critical angle. The mesostructure of the coating was further characterized by X-ray reflectometry (XRR). The experiments were performed at BL14B1 beamline of SSRF and 1W1A beamline of BSRF in China with the X-ray wavelength 0.124 nm and 0.154 nm, respectively. XRR data were recorded with θ-2θ scan mode and diffraction results were collected over the range of 0.2^o -4^o. The coating thickness can be calculated from the so-called Kiessig fringes based on the Parratt recursive formalism. The nitrogen ad/desorption technology was carried out at -196 ^oC on an ASAP 2020 instrument. The surface area found using Brunauer-Emmett-Teller formalism and the pore size distribution were calculated using a calculated Barret-Joyner-Halenda (BJH) model for the adsorption branch isotherm.

The transmission spectra of the AR coating was tested with UV-Vis spectrometer (lamda-950, Perkin Elmer), and the measured spectral range is from 300 nm to 1100 nm. The reflective index and physical thickness were measured by on a spectroscopic ellipsometer (SE 850, Sentech) at 70^o incidence, with a relative measurement error of about ±1 %.

The surface morphology of the coating was determined using an atomic-force microscopy (AFM, Nanoscope IV, Digital Instruments). Mechanical properties of the coatings were investigated using an instrumented nanoindenter XP (MTS) with a Berkovtich tip.

The Laser induced damage threshold (LIDT) of the coating was tested at a 1053 nm laser. The pulse width was 12 ns and the laser spot area was 1 mm^2. The R-on-1 testing mode was carried out at 40 different locations that were arranged into an 8×5 array. According to International Organization for Standardization standard ISO11254-2.1, the distance between two close spots was 5 mm, sufficient to prevent the spots from disturbing each other. The coatings were shot until damage occurred by increasing the irradiation energy from 0 to 0.5 mJ in one step. The damage morphology of the coating was estimated from the visual inspection of plasma flash and detected in situ with an interferential contrast microscope (Nikon E600W).

3. Results and discussion

3.1. The formation mechanism of mesopores in coating.

Ordered mesoporous silica coating in this work was synthesized using TEOS as precursor and F127 as structure director via evaporation-induced-self-assembly (EISA) process. As illustrated in Fig. 1, the whole preparation process was separated into two steps: the first step began with hydrolysis and polycondensation of TEOS in F127 solution with concentration far lower than the critical micelle concentration (cmc); the second step was the so-called EISA process to deposit coating on substrate.

Because F127 concentration was far lower than cmc, micelles cannot form in solution. On the other hand, hydrolyzed TEOS is soluble under acidic solution. Therefore, the transmissive SAXS technology cannot be used to investigate the first step mentioned above. However, the second step can be detected. During dip coating, the evaporation of ethanol and then water at air/film interface induced fast increase in concentrations of F127 and silica species. Once above the cmc, lots of micelles came into being, and the self-assembly of oligomeric silicious species began around the micelles. Finally, the polycondensation of TEOS formed the inorganic network of mesopores.[37] Here using GISAXS and XRR, we measured the structure evolution of as-prepared coating, dried coating for 24 h at room temperature, and, calcined coating at 550 ^oC to show the formation of mesopores.

Fig .2 shows GISAXS patterns of as-prepared, dried and calcined coating F05. It can be seen that as-prepared coating showed four clear Bragg diffraction spots (Fig. 2a), confirming the existence of ordered structure. The number of spots increased to six after drying 24 h (Fig. 2b), suggesting the drying process at room temperature was helpful to the further organization in coating. After calcination to remove the template, the diffraction spots became brighter (Fig. 2c),

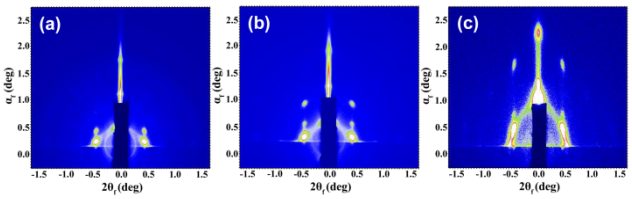

Fig. 2 GISAXS patterns of (a) as-prepared coating F05, (b) dried coating F05 and (c) calcined coating F05.

indicating the periodicity of mesostructure was improved. In addition, the pattern was elongated in the vertical direction, corresponding to the contraction in the direction vertical to substrate during the removal of the template. The XRR curves of as-prepared, dried and calcined coating F05 are shown in Fig. 3. One Bragg peak can be seen in the as-prepared coating (Fig. 3a), which corresponds to an initiatory periodic structure. After dried 24 h, the Bragg peak became stronger and narrower (Fig. 3b), suggesting the slightly improved ordering structure. Obviously different from the front samples, three Bragg peaks can be seen for the calcined coating (Fig. 3c), suggesting the existence of highly organized pores. From above analysis, the fundamental mesoscopic structure formed in the as-prepared coating after the substrate withdrawal from the solution. While drying, the ordering structure was improved. After thermal treatment, highly ordered mesopores were created in coating. The ordered structure of mesoporous silica coatings with various F127/TEOS molar ratio and different post-treatment were determined and explained in detail by followed GISAXS and XRR results.

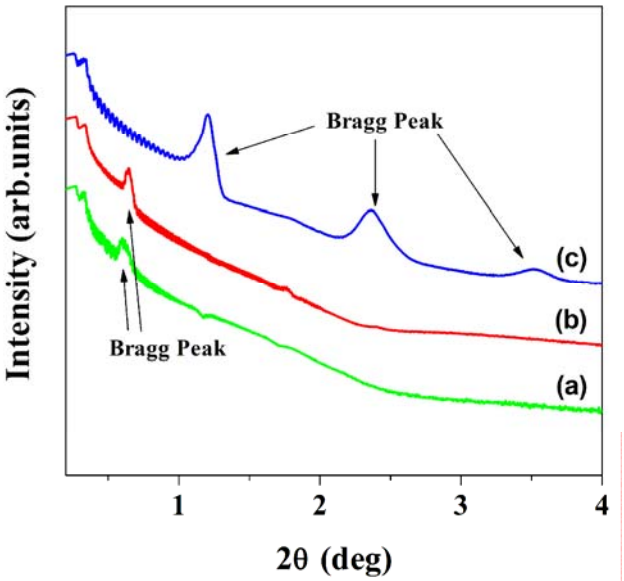

Fig. 3 XRR curves of (a) as-prepared coating F05, (b) dried coating F05 and (c) calcined coating F05.

3.2. The ordered structure determined from GISAXS and XRR.

Ordered mesopores in coating tend to orient with a specific (hkl) plane parallel to the substrate.[38] Generally speaking, it is difficult to identify the structure and lattice constants from traditional X-ray diffraction because coating always shows very limited diffraction peaks. Therefore at first 2D GISAXS was used to determine the mesostructure of coating, because it can reveal the most features of reciprocal space. At the grazing incidence angle, the effective sample volume for X-ray scattering becomes large and hence avoids the disturbance from substrates, which will result in strong scattering patterns from coating with only a few hundred nanometers.

The GISAXS images of the calcined mesoporous silica coatings are shown in Fig. 4. Bragg diffraction spots can be clearly observed from Fig. 4, confirming that the mesoporous silica coatings are highly organized. Interpretation of the GISAXS patterns was aided by NANOCELL,[39, 40] a Mathematica-based program that simulated quantitatively the

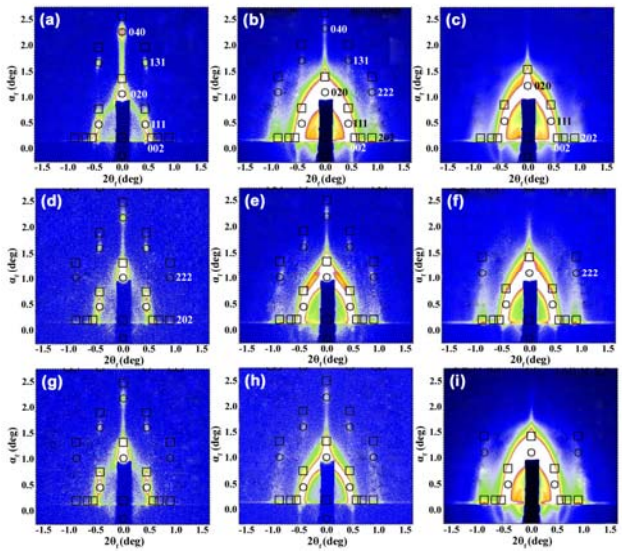

Fig. 4 2D GISAXS patterns of the calcined ordered mesoporous silica coatings with different surfactant content and different post-treatment (a) F05, (b) F07, (c) F09, (d) F05N, (e) F07N, (f) F09N, (g) F05NF, (h) F07NF and (i) F09NF. The overlay of simulated spots is from a NANOCELL software. The hollow circles and square identify transmitted and reflected Bragg peaks, respectively. Besides, the simulated results show the reciprocal space of an (010) oriented Fmmm space group.

positions of Bragg peaks at any incidence angle above the critical angle. This simulation program used the distorted wave Born approximation to account for the effects of refraction and reflection at coating-substrate and coating-air interfaces. The hollow circles and squares in the patterns represent the simulated transmissive and reflective spots respectively. The observed and simulated spots are in a good agreement and all the spots were fitted to a face-centered orthorhombic Fmmm structure with (010) planes parallel to the substrate. For the coating F05 (Fig. 4a), five diffraction spots are clearly observed and indexed to (020), (040), (111), (131) and (002) reflections of the Fmmm space group. Generally speaking, mesoporous silica coatings with 3D mesoporous structure can be synthesized using PEO-PPO-PEO block polymers as template with EO/PO group ratio higher than 1.5.[35] Similar ordered mesoporous silica coatings prepared using triblock copolymer F127 as a template have been reported in some literatures.[38, 41, 42] Referred to the phase diagrams of Pluronic F127,[43] a primitive cubic structure of Im3m symmetry should arise from the arrangement of spherical micelles. Therefore, the Fmmm mesostructure presented here should result from the uniaxial shrinkage along the substrate normal. With increasing the F127/TEOS molar ratio to 0.007 of the coating F07 (Fig. 4b), a diffraction ring appears in the image but the fundamental spot-like pattern can still be observed. Further increasing the surfactant content to 0.009 of the coating F09 (Fig. 4c), some diffraction spots disappear and the diffraction ring is more obvious than that of the coating F07. The diffraction ring is caused by the randomly oriented pore arrangement in coating and poor periodicity of mesopores.[44] The structure parameters of coating are shown in Table 1. The symbol b_{SAXS} was used to mark the lattice constant b obtained by GISAXS and NANOCELL fitting. The lattice constants of the coating F05 were determined to be a=20.5 nm, b_{SAXS}=11.8 nm and c=24.5 nm. From Table 1, with increasing the surfactant content, the constant b_{SAXS} decreased from 11.8 nm of F05 to 10.4 nm of F09, because higher surfactant content means larger contraction during calcination to remove template. However, the constants

Table 1 Structure parameters of ordered mesoporous silica coatings with various F127/TEOS molar ratio and different post-treatment.

Sample	GISAXS			XRR		Pore size [nm]	Surface area [m^2g^{-1}]	Pore volume [cm^3g^{-1}]
	a [nm]	b_{SAXS} [nm][a]	c [nm]	α_{fc} [o][b]	b_{XRR} [nm][c]			
F05	20.5	11.8	24.5	0.134	11.8	4.9	352.86	0.19
F07	20.5	11.5	24.5	0.126	11.5	4.9	478.26	0.22
F09	20.5	10.4	24.5	0.122	10.3	4.9	482.22	0.30
F05N	20.5	12.2	24.5	0.130	12.1	6.4	537.03	0.30
F07N	20.5	12.1	24.5	0.120	12.2	6.4	560.83	0.34
F09N	20.5	11.2	24.5	0.118	11.2	6.4	577.70	0.40
F05NF	20.5	12.2	24.5	0.130	12.2	/[d]	/	/
F07NF	20.5	12.1	24.5	0.120	12.2	/	/	/
F09NF	20.5	11.2	24.5	0.118	11.2	/	/	/

[a] b_{SAXS} is the constant b fitted from 2D GISAXS. [b] b_{XRR} is the constant b obtained from XRR. [c] α_{fc} is the coating critical angle from XRR. [d] "/" means that those parameters did not be measured because the fluoroalkyl-grafting has no effect on the pore structure.

a and c show no change, because the shrinkage of coating structure in the direction parallel to substrate has been hindered by the adhesion of coating.

The synthesis process of ordered mesoporous silica coatings involved the formation of organic-inorganic composites by an evaporation-induced-self-assembly in which the organic phase is organized on mesoscopic scale and serves as the template of inorganic skeleton. After calcination to remove surfactant, mesopores form in the coating. In most cases, mesoporous structure tends to collapse during heat-treatment especially in the present of vapor. To stiffen the inorganic network of silica coating, ammonia vapor was used as a condensation promoter to post-treated the fresh silica coating with template in it.[45,46] Fig. 4d-f show the GISAXS images of coatings F05N, F07N and F09N that are ammonia-treated coatings F05, F07 and F09. The three coatings show more diffraction spots than those pure coatings, suggesting ammonia treatment process is helpful to improve the ordered structure. Furthermore, ammonia-treated ordered mesoporous silica coatings have the larger lattice constant b_{SAXS} than those original coatings (seen in Table 1). Because ammonia vapor treatment process increased the density of silica network and decreased the contraction and collapse during calcination.

To prove the successful fluoroalkyl-grafting, X-ray photoelectron spectrometer survey spectra of coating F07N and F07NF are shown in Fig. S1 (Supporting Information), in which F07NF is the fluoroalkyl-grafted F07N. F1s symbol can be clearly observed in coating F07NF. Other fluoroalkyl-grafted coatings have similar results as F07NF, suggesting that fluoroalkyl groups have been successfully grafted on the surface of coating. Fig. 4g-i show the GISAXS images of the fluoroalkyl-grafted coatings F05NF, F07NF and F09NF. The GISAXS patterns of coatings have no obvious change after fluoroakyl-grafting. From Table 1, it also can be seen that fluoroalkyl-grafting process had no effect on the structural parameters of coating because the fundamental mesoporous skeleton of ammonia-treated coating has been solidified after 550 ^{o}C calcination for 1 h to remove the surfactant, and thus fluoroalkylsilane surface modification at 150 ^{o}C cannot affect the real structure.

The ordered structure of mesoporous silica coating was further confirmed by XRR. The XRR curves are shown in Fig. 5, in which Bragg peaks and Kiessig fringes are clear for all the samples. The presence of Bragg peaks shows the periodic structure, and, the Kiessig fringes results from the finite measurable thickness of coating.[47] For each coating, two critical angles can be observed in its XRR curve within the 2θ range of 0~0.5^{o}. The first one corresponds to the critical angle of coating, α_{fc}, and the second one is that of quartz glass substrate, α_{sc} constant 0.174^{o}. The α_{fc} values are shown in Table 1. The α_{fc} decreases from 0.134^{o} of F05 to 0.122^{o} of F09 and from 0.130^{o} of F05N to 0.118^{o} of F09N with increase the molar ratio of F127/TEOS, indicating the reduction of average electron density of coating caused by the increase of pores. As predicted, the α_{fc} of mesoporous silica coatings after fluoroalkyl-grafting did not change.

As can be seen in Fig. 5, three Bragg peaks in the 2θ range of 1^{o}-4^{o} can be clearly distinguished and indexed to the (020), (040) and (060) reflections of a face-centered orthorhombic structure for the samples F05, F07, F05N and F07N. According to the Fmmm symmetry, the lattice parameter b equals to $2d_{(020)}$. To show a difference from the b_{SAXS} obtained from the GISAXS result, b_{XRR} was used to mark the parameter b obtained from XRR curve as shown in Table 1. It is obvious

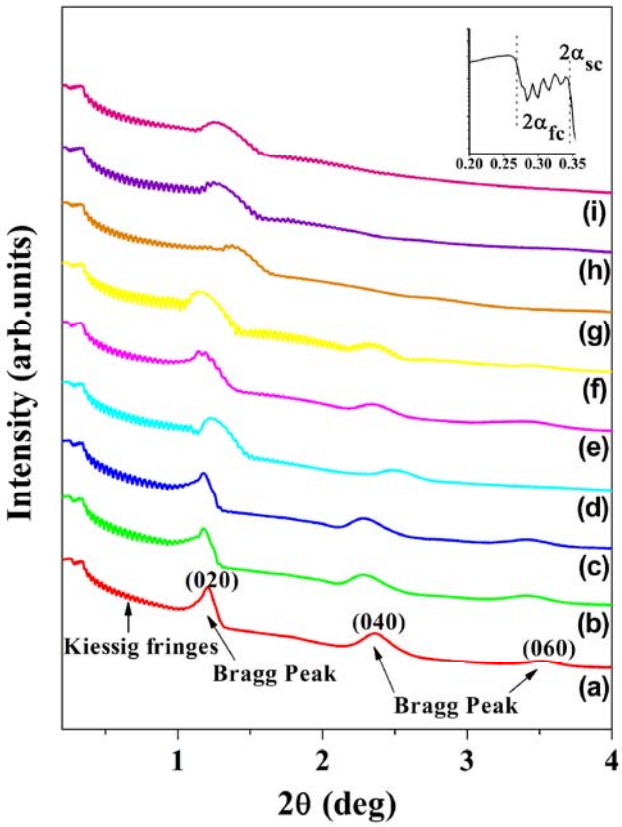

Fig. 5 XRR curves of the mesoporous silica coatings (a) F05, (b) F05N, (c) F05NF, (d) F07, (e) F07N, (f) F07NF, (g) F09, (h) F09N and (i) F09NF for various the molar ratios of F127/TEOS and different post-treatment. The top right inset shows a magnified view of the region around the critical angle. The α_{fc} is the critical angle of coating and the α_{sc} is the critical angle of substrate.

that the b_{XRR} values of coatings are in a good agreement with b_{SAXS}. As increasing the surfactant content, Bragg peaks were weakened and broadened, suggesting the ordering decreased (seen from Fig. 5a, 5d and 5g).

Seen from Table 1, each ammonia-treated coating has larger b_{XRR} than the pure coating. From Fig. 5, the Bragg peaks of ammonia-treated mesoporous silica coatings exhibit small shift towards lower angle, which is a characteristic of increased periodic length corresponding to the constant b_{XRR}. The reason has been discussed in the analysis of GISAXS result.

The fluoroalkyl-grafted mesoporous silica coatings have same b_{XRR} as their ammonia-treated counterparts in Table 1, which is also consistent with GISAXS results. Both GISAXS and XRR methods are complementary and allow for a very detailed characterization of coating structure.

3.3. The pore structure of coating.

Through nitrogen adsorption/desorption analysis, the pore structure information of coating was obtained on coating fragments scratched off substrate. The type-IV isotherm is shown in Fig. 6 for the coatings. Type-H_2 hysteresis loops appears between the relative pressure of 0.4 and 0.7 for the coating F05 (Fig. 6a), showing the existence of cage-like mesopores in coating.[35] With increasing the surfactant content to 0.007 of F07, despite a little shape change, type-H_2 hysteresis loop still exists, suggesting that cage-like mesopore was maintained in coating F07 (Fig. 6b). When the molar ratio

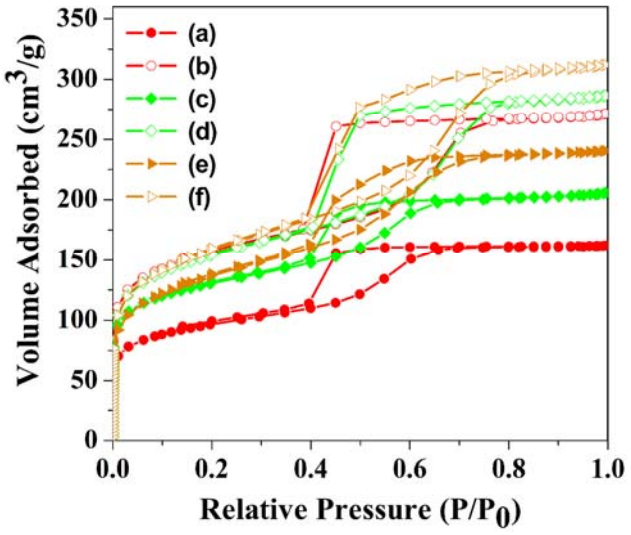

Fig. 6 Nitrogen adsorption-desorption isotherms measured at -196 °C for the samples (a) F05, (b) F05N, (c) F07, (d) F07N, (e) F09 and (f) F09N.

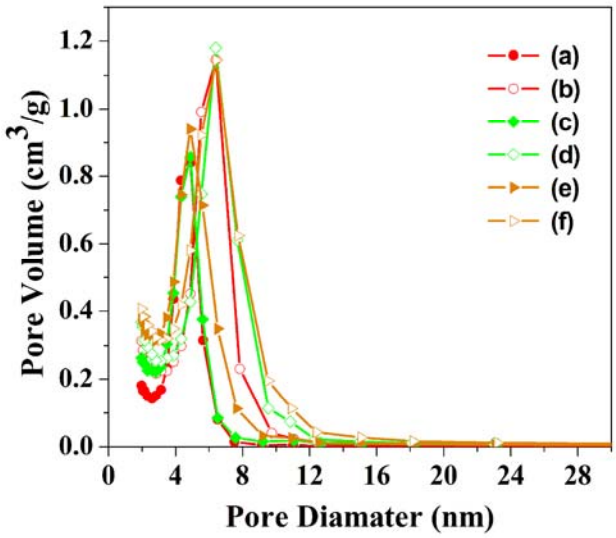

Fig. 8 Pore size distribution plots calculated using BJH model for the adsorption branch isotherm for the samples (a) F05, (b) F05N, (c) F07, (d) F07N, (e) F09 and (f) F09N.

of F127/TEOS reaches 0.009, the hysteresis loop of coating F09 deforms and displays a type-H_1 characterization (Fig. 6c),[48] suggesting the existence of some cylindrical mesopores. The appearance of cylindrical mesopores should be attributed to: (1) at first, relatively small amount of silica precursors were not enough to fully cover the surface of F127 micelles in F09 preparation; (2) then the entrances of cage-like mesopores became larger and the connectivity between pores was enhanced, which can be illustrated by the Fig. 7. As described in the Fig. 7, the effect of F127/TEOS ratio on pore structure can be found in surface area and pore volume shown in Table 1,

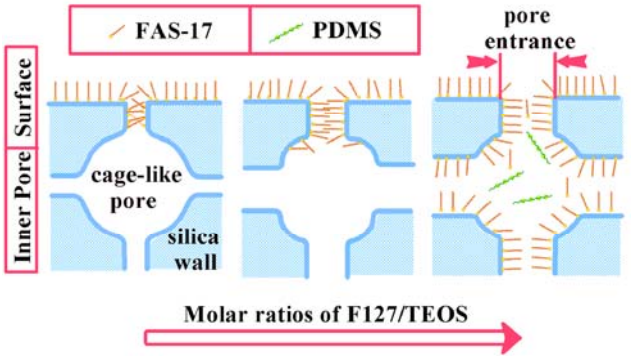

Fig. 7 Schematic illustration of changes in the cage-like pore structure brought about by increasing the F127/TEOS molar ratio. The speculation of fluoroalkyl-grafting on the surface or inside of the ordered mesoporous silica coatings and the influence of PDMS contamination.

the surface area and pore volume all increase from 352.86 m^2g^{-1} and 0.19 cm^3g^{-1} of F05 to 482.22 m^2g^{-1} and 0.30 cm^3g^{-1} of F09. However, also from Table 1, the mean pore size does not change with the F127/TEOS ratio. The pore size distribution plots of coating are shown in Fig. 8. The pore size is mainly decided by the nature of surfactant F127, that is, the size of F127 micelles in solution. Therefore, the pore sizes of pure mesoporous coatings F05, F07 and F09 are 4.9 nm.

For the ammonia-treated ordered mesoporous silica coatings, the hysteresis loops of coatings become larger than the pure ones, shown in Fig. 6d-f, indicating larger cage-like mesopores. Seen Table 1, the surface area of coating F05N reaches 537.03 m^2g^{-1} from 352.86 m^2g^{-1} of F05 and pore volume reaches 0.30 cm^3g^{-1} from 0.19 cm^3g^{-1} of F05. Similarly, the surface areas and the pore volumes of the other two ammonia-treated coatings are also higher than the pure ones. Ammonia treatment stiffened silica mesopore wall and consequently reduced the contraction and collapse of mesopores so that higher porosity was obtained after ammonia-treatment. Also from Table 1, the pore size of ammonia-treated coatings becomes larger than that of the pure ones. Because the Barret-Joyner-Halenda method which assumes cylindrical pore model was used to calculate pore size. The ammonia-treated mesoporous coatings have larger cage-like pores than pure coatings due to their smaller pore contraction during calcination.

The pore structure information are not provided for the fluoroalkyl-grafted mesoporous silica coatings and the corresponding spaces are marked as "/" in Table 1. Because fluoroalkylxane post-grafting process just went on the very surface of coating, amounts of the successful grafted are very limited. Once the fluoroalkyl-grafted coating was scratched off the substrate, no difference could be detected compared with the ungrafted coating.

3.4. Coating thickness.

The physical thickness of coating was obtained by fitting the Kiessig fringes in XRR curve and measured by spectroscopic ellipsometer.[49,50] The results obtained by two methods were marked as d_{XRR} and d_{EP} respectively as shown in Table 2. A good agreement between d_{XRR} and d_{EP} can be found, showing that the physical thickness is accurate. The thickness of coating have been adjusted to match the demand in antireflection at 1053 nm, therefore, they show little variation.

3.5. The optical property of coating.

The transmittance curves of ordered mesoporous silica coatings on quartz glass substrate are shown in Fig. S2 (Supporting Information) and the corresponding transmittance at wavelength 1053 nm, T_1, are collected in Table 2. The optical thickness of mesoporous coating was controlled to match the

Table 2 Parameters of ordered mesoporous silica AR coatings with various F127/TEOS molar ratio.

Sample	n_f [a]	d_{EP} [nm][b]	d_{XRR} [nm][c]	Rq [nm][d]	E [Gpa][e]	LIDT [Jcm^{-2}][f]	T_1 [%][g]	T_2 [%][h]	ΔT [%][i]
F05	1.295	203.6	203.8	1.8	36.47	53.59	99.02	98.45	0.57
F05N	1.249	211.7	212.1	1.2	37.51	54.05	99.69	99.09	0.60
F05NF	1.249	212.4	212.9	2.3	37.51	54.74	99.71	99.69	0.02
F07	1.244	212.0	211.9	1.3	26.52	57.96	99.74	98.78	0.96
F07N	1.223	215.6	216.0	0.8	36.39	58.40	99.98	98.95	1.03
F07NF	1.226	216.1	216.7	1.4	36.40	59.80	99.94	99.88	0.06
F09	1.220	216.5	216.1	0.8	24.12	56.12	99.99	98.81	1.18
F09N	1.214	217.6	218.3	0.9	20.70	57.50	100.00	98.73	1.27
F09NF	1.243	217.8	218.2	0.8	20.72	57.73	99.74	99.47	0.27

[a] n_f is the refractive index of coating. [b] d_{EP} is the thickness of coating measured by ellipsometer. [c] d_{XRR} is the coating thickness calculated from XRR. [d] Rq is the root-mean-square roughness of coating. [e] E is elastic modulus. [f] The LIDT is the laser-induced damage threshold. [g,h] T_1 and T_2 are respectively the transmittances at 1053 nm before and after an one-month test in PDMS vapor, and, the measurement error is ± 0.01 determined by the UV-Vis spectrometer. [i] $\Delta T = T_2 - T_1$.

desired antireflective wavelength 1053 nm by adjusting the dip-coating speed. The transmittance of quartz substrate at 1053 nm was about 93 %. With coating, the transmittance of element at 1053 nm was enhanced at least 6 % compared to bare quartz substrate. The transmittance increases from 99.02 % of F05 to 99.99 % of F09 with increasing the surfactant content. The ammonia-treated coatings have obviously higher transmittance than the pure coatings. For the coating F09N, the transmittance reached 100.00 %, the best AR performance. The transmittance of fluoroalkyl-grafted coatings showed little change compared with the ungrafted coatings, except for the coating F09NF. The transmittance at 1053 nm decreases from 100.00 % of F09N to 99.74 % of F09NF after fluoroalkyl-grafting.

Optimum optical performance of single layer AR coating can be achieved by following the principle: $n_f = (n_a \times n_s)^{0.5}$, where n_f , n_a and n_s are refractive indexes of AR coating, air and substrate, respectively.[51] Refractive index and thickness of mesoporous silica coating was measured with ellipsometer and shown in Table 2. When the F127/TEOS molar ratio increases, the refractive index of coating decreases from 1.295 of F05 to 1.220 of F09 because more and more mesopores were formed. Ammonia-treated coatings F05N and F07N have the lower refractive index than pure mesoporous coating, seen from Table 2, suggesting ammonia treatment strengthens the silica skeleton and reduces the possibility of pore collapse during calcination. For the coating F09N, the refractive index has little changed, showing little effect of ammonia treatment. As higher surfactant content means less silica in coating, the contraction of silica skeleton is smallest in F09N. Also seen from Table 2, there is a small increase in refractive index of the coating: from 1.223 of F07N to 1.226 of F07NF. The thicknesses of F07N and F07NF are almost same. However, after fluoroalkyl-grafting, the refractive index of the coating F09N increases from 1.214 to 1.243 of F09NF, and, the physical thickness remains almost constant. The decrease in transmittance of the coating F09NF accompanied with the increase in refractive index can be attributed to that more fluoroalkyl groups have been grafted into pore channels. Seen from Fig. 7, high surfactant content in precursor solution enhanced the connectivity between cage-like mesopores, thus more FAS-17 molecules will transfer into the pore channels during fluoroalkyl-grafting process for F09N and resulted in lower transmittance. But for other samples, the grafted fluoroalkyl groups should be mainly distributed on the mesopore openings and show ignorable effect on transmittance.

3.6. The surface morphology and elastic modulus of coating. The typical morphology and surface roughness of ordered

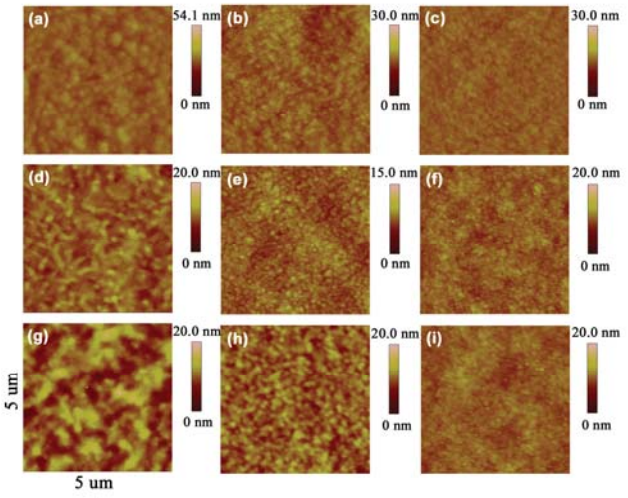

Fig. 9 AFM images of ordered mesoporous silica AR coatings with various surfactant content (a) F05, (b) F07, (c) F09, (d) F05N, (e) F07N, (f) F09N, (g) F05NF, (h) F07NF and (i) F09NF.

mesoporous silica coatings were tested by AFM. The AFM images and root-mean-square roughness, Rq, of all the coatings are shown in Fig. 9 and Table 2, specifically, there are many particle-like bumps on the surface of the coating F05 (Fig. 9a), and the Rq is 1.8 nm. With increasing the F127/TEOS molar ratio, coating surface becomes smoother, and Rq decreases to 0.8 nm of F09 (Fig. 9c), resulted from more condensation Si-OH groups in the case of low surfactant content. For ammonia-treated mesoporous coatings, no cracks can be seen on coating surface while massive small particles emerge (Fig. 9d-f), indicating ammonia treatment promoted the condensation of Si-OH groups.[43] After fluoroalkyl-grafting, the Rq of coatings F05N and F07N increase, while the Rq of the coating F09N has very small decrease. From above coating surface roughness, the coatings are all smooth enough to avoid surface scattering that is harmful for antireflection.

Elastic modulus is an important parameter to evaluate the ability of porous material to withstand stress-induced deformation. Porosity, pore orientation, thickness and density of pore wall are the most dominating factors for the mechanical property of porous materials.[52-56] The elastic modulus of mesoporous silica coating is shown in Table 2. As can be seen, the elastic modulus of pure coating decreases from 36.47 GPa of F05 to 24.12 GPa of F09, and, the elastic modulus of ammonia-treated coatings also decreases from 37.51 GPa of F05N to 20.70 GPa of F09N with increase the F127/TEOS molar ratio. Thus degradation in mechanical properties is mainly caused by the increase in porosity seen the pore volume in Table 1. For ammonia-treated mesoporous coatings F05N and F07N have obviously larger elastic modulus than the pure coatings mainly due to the increase in density of silica network. However, the lowest elastic modulus of coating F09N may be caused by the highest porosity. The elastic modulus of fluoroalkyl-grafted coating is same as that of ammonia-treated coating. In general, the mechanical performance of ordered mesoporous silica coating is superior to the traditional base-catalysed sol-gel porous silica coatings ranging from 2.38~5.02 GPa.[57] The base-catalysed porous sol-gel silica coatings can be easily irreversibly damaged when physically toughed or wiped because the binding force between silica particles and substrate is quite weak as well as between particles in coating. However, the ordered mesoporous silica coating prepared in acidic catalysis condition has strongly cross-linked pore framework and good adhesion with substrate, thus the coating possess strong scratch resistance.

3.7. The laser induced damage of coating.

Laser induced damage of optical coatings is a serious problem in high power laser system and especially in vacuum where various contaminants can be present. The LIDT values of the ordered mesoporous silica coatings are also shown in Table 2. As can be seen, all LIDT of the coatings are over 53 Jcm^{-2} at 12 ns in 1053 nm laser. The difference in LIDT between coatings was not obvious enough to show some defined relations between LIDT and the surfactant content or ammonia-treatment or fluoroalky-grafting process. The typical damage morphology of the coating F07NF is shown in Fig. 10. The damage center is molten coating and three circles can be observed around the damage spot, which is typical fusion damage. The size of the damage spot is about 100 μm. No delamination damage or plasma scald damage was observed in the coating. Other coatings show similar damage morphology.

3.8. The stability of coating in vacuum.

It seems true that space is clean in high vacuum because volatile matter cannot be adsorbed on the walls of vacuum chamber. However, in the vacuum chamber of high power lasers, many nonvolatile organic matters can be vaporized under the large negative pressure of high vacuum and become troublesome contaminants for optical elements in vacuum. The adsorption of contaminants in vacuum systems reduces the optical transmittance and LIDT of AR coatings, which severely influence the normal running of laser system. For this purpose, we compared the environment stability of ordered mesoporous silica coatings before and after fluoroalkyl-grafting. Only two typical coatings F07N and F07NF were discussed here because of their excellent transmittance and the highest LIDT. The transmittance curves of F07N and F07NF before and after stability test are shown in Fig. 11 after exposure to PDMS vapor in 10^{-3} Pa vacuum for 1 month. The transmittance of the coating F07N has an obvious decrease from 99.98 % to 98.95 %, while the coating F07NF has a small decrease from 99.94 % to 99.88 %, suggesting fluoroalkyl-grafting process can largely improve the stability of ordered mesoporous silica AR coating in vacuum. The detailed effect of closed pore structure on the antipollution of AR coatings in vacuum can be described by $\Delta T=T_2-T_1$ in Table 2. The parameter T_2 shows the transmittances at 1053 nm wavelength of ordered mesoporous silica AR coatings after a one-month test in PDMS vapor under vacuum of 10^{-3} Pa. After this one-month antipollution test, the smallest decrease in transmittance, 0.02 %, can be found in coating F05NF, while the decrease of coating F05N is up to 0.6 %. The ΔT becomes larger with increasing the surfactant content. When the F127/TEOS molar ratio is 0.009, the ΔT of F09N is high as 1.27 %, but for the fluoroalkyl-grafted coating F09NF, the ΔT is only 0.27 %. In addition, whether the ordered mesoporous coatings undergo fluoroalkyl-grafting or not, the absolute value of ΔT data increases with increasing the surfactant content, which should be caused by the enlargement of the pore entrance of the mesoporous coatings resulting in stronger adsorption of PDMS molecules. From the ΔT data in Table 2, fluoroalkyl-grafted coatings show better stability in vacuum, which indicates most of open mesopores have been "closed" after fluoroalkyl-grafting. Considering the molecular length 1.33 nm of FAS-17, as the surfactant content increased, long-chain FAS-17 molecules cannot completely close the entrance of mesopores, e.g. in the sample F09NF, some PDMS molecules can still get into pores in antipollution test (see Fig. 7). Thus ΔT of coating F09NF is biggest. In a word, the

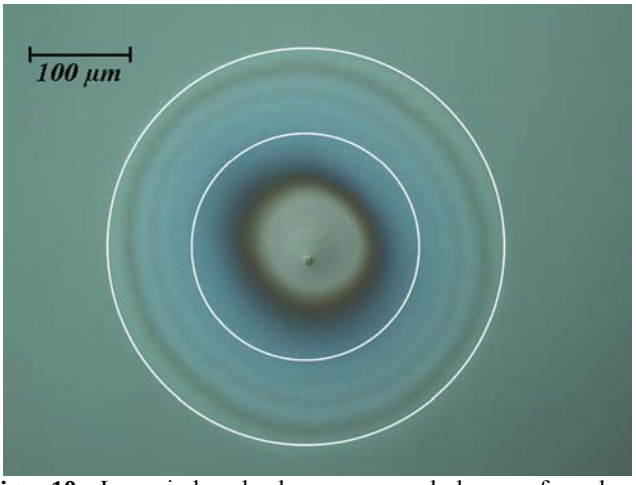

Fig. 10 Laser-induced damage morphology of ordered mesoporous silica coating F07NF.

fluoroalkyl-grafting process can significantly improve the stability of ordered mesoporous silica AR coatings in vacuum.

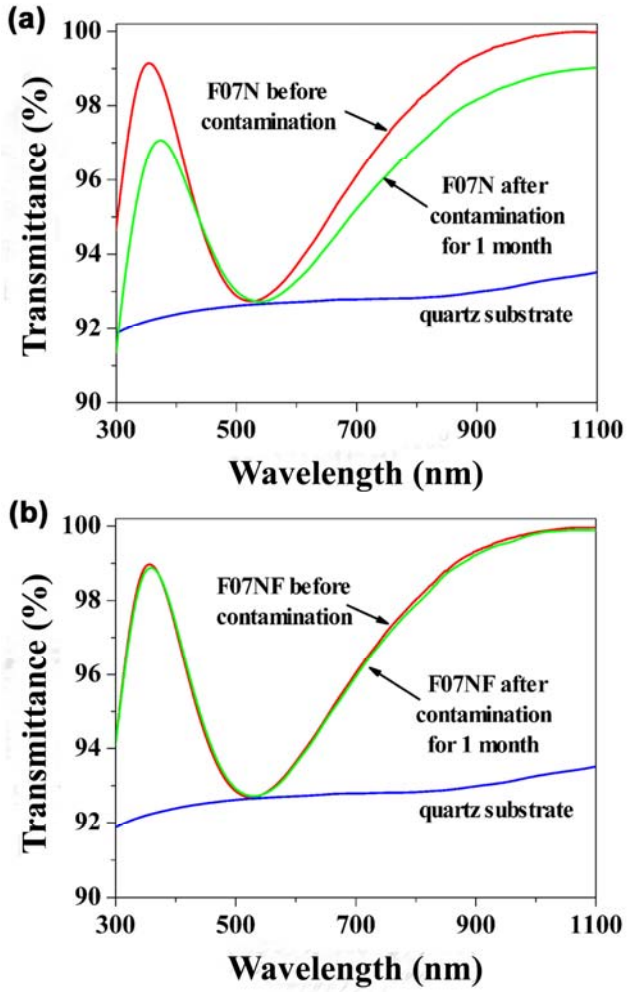

Fig. 11 Transmittance of ordered mesoporous silica AR coatings (a) F07N and (b) F07NF before and after exposure to PDMS vapor under 10^{-3} Pa vacuum for a month.

4. Conclusions

In summary, a contamination-resistant optical AR coating with face-center orthorhombic symmetry and closed cage-like mesoporous structure have been successfully prepared for high power laser system. The coatings possessed excellent transmittances, high LIDT, strong mechanical properties and good vacuum stability. In addition, the closed pore structure of ordered mesoporous coatings by post-grafting the long chain fluoroalkylsilane on the surface pore entrance provides a good method for improving AR coating stability. The ordered mesoporous silica coating with closed mesopores, F07NF, is a good candidate for the future application of AR coating in vacuum of high power lasers.

Acknowledgements

This work was supported by the National Key Native Science Foundation, China (No.10835008) and National Science Foundation of Shanxi (No. 2012011005-1).The authors wish to acknowledge the BL14B and BL16B beamlines of SSRF and 1W1A and 1W2A beamlines of BSRF in China. Additionally, the authors gratefully acknowledge the assistance of Prof. Hugh W. Hillhouse and Dr. Steve Gaik of University of Washington during the analysis of GISAXS patterns.

Notes

[a] Key Laboratory of Carbon Materials, Institute of Coal Chemistry, Chinese Academy of Sciences, Taiyuan 030001, China.
[b] University of Chinese Academy of Sciences, Beijing 100049, China.
[c] Research Center of Laser Fusion, China Academy of Engineering Physics, Mianyang 621900, China.

*Corresponding author, e-mail: xuyao@sxicc.ac.cn

Electronic Supplementary Information (ESI) available: [details of any supplementary information available should be included here]. See DOI: 10.1039/b000000x/

References

1 J. Moghal, J. Kobler, J. Sauer, J. Best, M. Gardener, A. A. R. Watt and G. Wakefield, *ACS Appl. Mater. Interfaces*, 2012, **4**, 854-859.
2 L. G. Xu and J. H. He, *J. Mater. Chem. C*, 2013, **1**, 4655-4662.
3 C. S. Thompson, R. A. Fleming and M. Zou, *SOL ENERG MAT SOL C*, 2013, **115**, 108-113.
4 H. G. Floch and P. F. Belleville, *Proc. SPIE*, 1994, **2253**, 764-790.
5 D. R. Uhlmann, J. M. Boulton, G. T. Teowee, L. Weisenbach and B. J. Zelinski, *Proc. SPIE*, 1990, **1328**, 270-295.
6 Y. Xu, L. Zhang, D. Wu, Y. H. Sun, Z. X. Huang, X. D. Jiang, X. F. Wei, Z. H. Li, B. Z. Dong and Z. H. Wu, *J. Opt. Soc. Am. B*, 2005, **22**, 905-912.
7 X. G. Li, M. Gross, B. Oreb and J. Shen, *J. Phys. Chem. C*, 2012, **116**, 18367-18371.
8 B. Xiao, B. B. Xia, H. B. Lv, X. X. Zhang and B. Jiang, *J Sol-Gel Sci Technol*, 2012, **64**, 276-281.
9 X. X. Zhang, S. Cai, D. You, L. H. Yan, H. B. Lv, X. D. Yuan and B. Jiang, *Adv. Func. Mater.*, 2013, **23**, 4361-4365.
10 W. Stöber, A. Fink and E. Bohn, *J. Colloid Interface Sci.*, 1968, **26**, 62-69.
11 I. M. Thomas, *Appl. Opt.*, 1992, **31**, 6145-6149.
12 X. D. Wang and J. Shen, *J Sol-Gel Sci Technol*, 2012, **61**, 206-212.
13 H. A. Abdeldayem, E. Dowdye, J. Canham and T. Jaeger, *SPIE*, 2005, **5897**, 44-56.
14 R. Pareek, M. N. Kumbhare, C. Mukherjee, A. S. Joshi and P. D. Gupta, *Opt. Eng.*, 2008, **47**, 023801-1-023801-5.
15 G. M. Wu, J. Wang, J. Shen, T. H. Yang, Q. Y. Zhang, B. Zhou, Z. S. Deng, F. Bin, D. P. Zhou and F. S. Zhang, *J. Non-Cryst Solid*, 2000, **275**, 169-174.
16 H. P. Ye, X. X. Zhang, Y. L. Zhang, L. Q. Ye, B. Xiao, H. B. Lv and B. Jiang, *SOL ENERG MAT SOL C*, 2011, **95**, 2347-2351.
17 C. H. Chen, S. Y. Li, A. S. Chiang, A. T. Wu and Y. S. Sun, *SOL ENERG MAT SOL C*, 2011, **95**, 1694-1700.
18 Y. Xu, W. H. Fan, Z. H. Li, D. Wu and Y. H. Sun, *Appl. Opt.*, 2003, **42**, 108-112.
19 X. G. Li and J. Shen, *J Sol-Gel Sci Technol*, 2011, **59**, 539-545.

20 Y. Liu, J. Shen, B. Zhou, G. M. Wu and Z. H. Zhang, *J Sol-Gel Sci Technol*, 2013, **68**, 81-87.
21 X. X. Zhang, H. P. Ye, B. Xiao, L. H. Yan, H. B. Lv, B. Jiang, *J. Phys. Chem. C*, 2010, **114**, 19979-19983.
22 M. J. Mosquera, D. M. Santos and T. Rivas, *Langmuir*, 2010, **26**, 6737-6745.
23 X. M. Jiang and C. J. Brinker, *J. Am. Chem. Soc.*, 2006, **128**, 4512-4513.
24 A. L. Pénard, T. Gacoin and J.P. Boilot, *Acc. Chem. Res.*, 2007, **40**, 895-902.
25 R. A. Pai and J. J. Watkins, *Adv. Mater.*, 2006, **18**, 241-245.
26 L. Malfatti, P. Falcaro, D. Marongiu, M. F. Casula, H. Amenitsch and P. Innocenzi, *Chem. Mater.*, 2009, **21,** 4846-4850.
27 M. A. Norton, C. J. Stolz, E. Donohue, W. G. Hollingsworth, K. Listiyo, J. A. Pryatel and R. P. Hackel, *Proc. SPIE*, 2005, **5991**, 59910O-1-59910O-11.
28 G. Guéhenneux, P. Bouchut, M. Veillerot, A. Pereira and I. Tovena, *Proc.SPIE*, 2005, **5991**, 59910F-1-59910F-11.
29 H. Yang, A. Kuperman, N. Coombs, S. M. Afara and G. Ozin, *Nature*, 1996, **379**, 703-705.
30 D. Y. Zhao, J. L. Feng, Q. S. Huo, N. Melosh, G. H. Fredrickson, B. F. Chmelka and G. D. Stucky, *Science*, 1998, **279**, 548-552.
31 J. Kobler, K. Möller and T. Bein, *ACS Nano*, 2008, **2**, 791-799.
32 Z. G. Teng, G. F. Zheng, Y. Q. Dou, W. Li, C. Y. Mou, X. H. Zhang, A. M. Asiri and D. Y. Zhao, *Angew.Chem. Int. Ed.*, 2012, **51**, 2173-2177.
33 J. Wei, H. Wang, Y. H. Deng, Z. K. Sun, L. Shi, B. Tu, M. Luqman and D. Y. Zhao, *J. Am. Chem. Soc.*, 2011, **133**, 20369-20377.
34 J. Hwang and H. Daiguji, *Langmuir*, 2013, **29**, 2406-2411.
35 D. Y. Zhao, P. D. Yang, N. Melosh, J. L. Feng, B. F. Chemelka and G. D. Stucky, *Adv. Mater.*, 1998, **10**, 1380-1385.
36 R. Grudzien, M. S. Pikus and M. Jaroniec, *J. Phys. Chem. B*, 2006, **110**, 2972-2975.
37 D. Gross, A. R. Balkenende, P. A. Albouy, A. Ayral, H. Amenitsch and F. Babonneau, *Chem. Mater.*, 2001, **13**, 1848-1856.
38 S. Tanaka, Y. Katayama, M. P. Tate, H. W. Hillhouse and Y. Miyake, *J. Mater. Chem.*, 2007, **17**, 3639-3645.
39 M. P. Tate, V. N. Urade, J. D. Kowalski, T. C. Wei, B. D. Hamilton, B. W. Eggiman and H. W. Hillhouse, *J. Phys. Chem. B*, 2006, **110**, 9882-9892.
40 T. C. Wei and H. W. Hillhouse, *Langmuir*, 2007, **23**, 5689-5699.
41 P. Falcaro, D. Gross, H. Amenitsch and P. Innocenzi, *J. Phys. Chem. B*, 2004, **108**, 10942-10948.
42 S. Besson, C. Ricolleau, T. Gacoin, C. Jacquiod and J. P. Boilot, *Microporous and Mesoporous Materials*, 2003, **60**, 43-49.
43 Y. K. Hwang, K. R. Patil, S. H. Jhung, J. S. Chang, Y. J. Ko and S. E. Park, *Microporous and Mesoporous Materials*, 2005, **78**, 245-253.
44 E. K. Richman, T. Brezesinski and S. H. Tolbert, *Nat. Mater.*, 2008, **7**, 712-717.
45 N. Kitazawa, H. Sato and Y. Watanabe, *J Mater Sci*, 2007, **42**, 5074-5079.
46 D. Gross, A. R. Balkenende, P. A. Albouy, A. Ayral, H. Amenitsch and F. Babonneau, *Chem. Mater.*, 2003, **13**, 1848-1856.
47 S. Dourdain, J. F. Bardeau, M. Colas, B. Smarsly, A. Mehdi, B. M. Ocko and A. Gibaud, *Appl. Phys. Lett.*, 2005, **86**, 113108-113108-3.
48 P. J. Branton, P. G. Hall, K. S. W. Sing, H. Reichert, F. Schüth and K. K. Unger, *J. Chem. Soc.*, 1994, **90**, 2965-2967.
49 M. J. Henderson, A. Giband, J. F. Bardeau and J. W. White, *J. Mater. Chem.*, 2006, **16**, 2478-2484.
50 M. Henderson, J. K. Zimny, J. L. Blin, N. Delorme, J. F. Bardeau and A. Gibaud, *Langmuir*, 2010, **26**, 1124-1129.
51 A. Vincent, S. Babu, E. Brinley, A. Karakoti, S. Deshpande and S. Seal, *J. Phys. Chem. C*, 2007, **111**, 8291-8298.
52 S. B. Jung and H. H. Park, *Thin Solid Films*, 2006, **494**, 320-324.
53 W. Shimizu and Y. Murakami, *ACS Appl. Mater. Interfaces*, 2010, **2**, 3128-3133.
54 Y. Zhu, T. E. Muller and J. A. Lercher, *Adv. Func. Mater.*, 2008, **18**, 3427-3433.
55 H. Y. Fan, C. Hartshorn, T. Buchheit, D. Tallant, R. Assink, R. Simpson, D. J. Kissel, D. J. Lacks, S. Torquato and C. J. Brinkee, *Nat. Mater.*, 2007, **6**, 418-423.
56 F. Guillemot, A. B. Bruneau, E. Bourgeat-Lami, T. Gacoin, E. Barthel and J. P. Boilot, *Chem. Mater.*, 2010, **22**, 2822-2828.
57 A. Vincent, S. Babu and S. Seal, *Appl. Phys. Lett.*, 2007, **91**, 161901-161901-3.